AGU PUBLICATIONS

JGR

Journal of Geophysical Research: Atmospheres

RESEARCH ARTICLE
10.1002/2016JD026194

Key Points:
- Organic carbon concentrations follow different seasonal trends than black carbon in the Arctic
- Brown carbon light absorption is most efficient in the fall, which coincides with higher contributions of fossil carbon in select samples
- Radiocarbon abundance shows decreased fossil carbon contributions and increased biogenic contributions to organic carbon for spring and summer

Supporting Information:
- Supporting Information S1

Correspondence to:
R. J. Sheesley,
rebecca_sheesley@baylor.edu

Citation:
Barrett, T. E., and R. J. Sheesley (2017), Year-round optical properties and source characterization of Arctic organic carbon aerosols on the North Slope Alaska, *J. Geophys. Res. Atmos.*, *122*, 9319–9331, doi:10.1002/2016JD026194.

Received 4 NOV 2016
Accepted 9 AUG 2017
Accepted article online 14 AUG 2017
Published online 4 SEP 2017
Corrected 7 NOV 2017

This article was corrected on 7 NOV 2017. See the end of the full text for details.

Year-round optical properties and source characterization of Arctic organic carbon aerosols on the North Slope Alaska

T. E. Barrett[1] **and R. J. Sheesley**[1,2]

[1]The Institute of Ecological, Earth, and Environmental Sciences, Baylor University, Waco, Texas, USA, [2]Department of Environmental Science, Baylor University, Waco, Texas, USA

Abstract Long-term data on organic aerosol concentration and optical properties are needed in the Arctic to improve characterization of radiative forcing by atmospheric aerosols. This study presents the seasonal trends (summer 2012 to summer 2013) of organic carbon (OC) and water-soluble organic carbon (WSOC) along with optical properties of light-absorbing OC from a yearlong sampling campaign in Utqiaġvik, AK. Ambient OC concentrations for the year range from 0.008 ± 0.002 μg m^{-3} to 0.95 ± 0.06 μg m^{-3} with peaks in late summer, early fall, and late winter. On average, WSOC accounted for 57 ± 11% of the total OC burden throughout the sampling campaign, which is consistent with previous WSOC values. In order to understand the potential radiative impacts of light-absorbing OC, the light absorption properties of WSOC were determined. Seasonal averaging revealed that the highest average mass absorption efficiency value of 1.54 ± 0.75 m^2 g^{-1} was in the fall, with an annual range of 0.70 ± 0.44 to 1.54 ± 0.75 m^2 g^{-1}. To quantify the contributions of fossil and contemporary carbon sources to OC, radiocarbon abundance measurements were performed. For OC, fossil contributions were the greatest for select samples in the fall at 61.4 ± 9.8%, with contemporary contributions dominating OC in the spring and summer (68.9 ± 9.8% and 64.8 ± 9.8%, respectively). Back trajectories identified five major source regions to Utqiaġvik throughout the year, with a marine influence from the Arctic Ocean potentially present in all seasons. All these results point to impact from primary and secondary sources of OC in the Arctic.

Plain Language Summary In this study, trends and sources of atmospheric organic aerosols, or small particles in the atmosphere, are explored in the North American Arctic region (i.e., within the Arctic Circle). Organic aerosols can absorb sunlight and heat the atmosphere, cause snow and ice surfaces to darken, and act as seed particles for cloud formation. Aerosol samples were collected from summer 2012 to summer 2013 and analyzed to determine the sources of the particles: fossil fuel combustion (i.e., burning natural gas flares, diesel, or coal), biomass combustion (the burning of grass, trees, or biofuels), and biogenic emissions (aerosols derived from marine and terrestrial plant emissions). It was determined that fossil fuel combustion was an important source of aerosols in the fall, while nonfossil sources of organic aerosols, including biogenic emissions and biomass combustion events, were dominant in the spring and summer. Major source regions of these aerosols to the North American Arctic include the Russian Arctic, Canadian Arctic, the Alaskan Arctic, the Arctic Ocean, and western interior Alaska. This study highlights the potential climatic effects of light-absorbing organic aerosols and their sources in the North American Arctic and can be useful for determining climate mitigation strategies in this region.

1. Introduction

While the annual concentration and radiative impacts of some aerosol components, such as sulfate and black carbon (BC) have been studied extensively in the Arctic, organic carbon (OC) is not as well monitored or modeled, and little is known about the possible seasonal variability of OC. There are several established monitoring sites across the Arctic which have produced long-term BC trends: Svalbard, Norway; Alert, Canada; Utqiaġvik (formerly known as Barrow), AK, USA; and Summit, Greenland [*Bodhaine*, 1995; *Delene and Ogren*, 2002; *Eleftheriadis et al.*, 2009; *Hirdman et al.*, 2010; *Sharma et al.*, 2004; *Sharma et al.*, 2006; *Sharma et al.*, 2013]. However, there is limited information on seasonal OC characterization at those same sites [*Shaw et al.*, 2010]. In the Arctic, primary OC will be coemitted from the same combustion sources as BC but will also be emitted from marine and terrestrial biogenic sources and be produced from secondary reactions of anthropogenic and biogenic volatile organic carbon precursors [*Sharma et al.*, 2012]. A previous study

which focused on the wintertime OC and BC apportionment for particulate matter less than 10 μm (PM_{10}) at Utqiaġvik, AK, during the 2012–2013 campaign, found that the OC was significantly less fossil than BC [*Barrett et al*., 2015]. The current study will focus on PM_{10} OC concentration, sources, and optical properties from an annual campaign at Utqiaġvik, AK, for 2012–2013, enabling comparison with the long-term BC trends available for that site.

Arctic OC could impact the radiative balance via direct and indirect effects, but there is still uncertainty associated with quantifying these effects. Light-absorbing organic carbon, or brown carbon (BrC), has been shown to be responsible for up to 28% of total light absorption in California and for up to 50% of the total light absorption for biomass burning aerosols [*Bahadur et al*., 2012; *Chen and Bond*, 2010; *Kirchstetter et al*., 2004]. Recent modeling suggests that BrC contributes up to +0.25 W m^{-2} globally to the Earth's radiative budget (19% of the total absorption due to anthropogenic aerosols) and that the global atmospheric burden of BrC is more than 3 times the burden of BC [*Feng et al*., 2013]. Emissions of BrC have been attributed to both primary sources (biomass burning, residential heating by wood and coal, and biogenic emission) and secondary sources (high-molecular weight light-absorbing compounds produced in atmospheric reactions) [*Laskin et al*., 2015]. BC absorption exhibits little wavelength dependence across the UV-vis spectrum. In contrast, BrC absorption exhibits a strong wavelength dependence with higher absorption efficiency in the UV spectral region [*Srinivas and Sarin*, 2014]. Light absorption in the ultraviolet range is also of significance because it may affect photolysis rates of gaseous compounds in the atmosphere by decreasing the amount of total incoming solar radiation, leading to reduced tropospheric concentrations of atmospheric oxidants such as ozone [*Chen and Bond*, 2010; *Laskin et al*., 2015]. In terms of the indirect effect, the water soluble fraction of organic carbon (WSOC) may be important due to its ability to increase the hygroscopicity of particles and enable them to act as cloud condensation nuclei; WSOC can account for 20–70% of total organic aerosol mass [*Kirillova et al*., 2014]. While multiple techniques have been used to determine the presence and absorption properties of atmospheric BrC, the measurement of light absorption of liquid extracts of aerosol samples is a common method to determine the absorption properties of atmospheric BrC [*Chen and Bond*, 2010; *Cheng et al*., 2011; *Kirillova et al*., 2014] and is utilized for PM_{10} samples in this study. Previous size-resolved studies of absorption of aqueous extracts of PM_{10} and $PM_{2.5}$ samples showed that there was no significant difference in absorption between the two size fractions in remote regions of the Tibetan Plateau [*Li et al*., 2016].

As mentioned previously, long-term trends in OC, WSOC, and BrC have not been as well characterized across the Arctic. Prior to this study, the only long-term collection of atmospheric organic carbon samples was in northern Finland from September 1997 to June 1999 [*Ricard et al*., 2002] and in Utqiaġvik in 2008–2009, with gaps in analysis at midsummer and midwinter [*Shaw et al*., 2010]. Long-term studies of methanesulfonic acid (MSA, 1998–2008), a secondary product of the marine production of dimethyl sulfide, provide an understanding of decadal trends in secondary marine biogenic aerosol [*Quinn et al*., 2009; *Sharma et al*., 2012]. However, with increasing temperature, thinning ice, and decreasing ice extent, there is a need to project these trends into the future of the Arctic. Studies of seasonal trends in ambient concentration, absorption properties, and sources are needed to understand potential climate impacts of these aerosols and the impact of climate change on aerosol production [*Anderson et al*., 2008; *Hu et al*., 2013; *Kawamura et al*., 2010; *Shaw et al*., 2010].

This manuscript reports the results of an annual study (June 2012 to June 2013) of non-BC carbonaceous aerosols (OC, WSOC, and BrC) including seasonal trends in optical properties, ambient concentrations, and sources for Utqiaġvik, Alaska. Multiple off-line analytical techniques for non-BC carbon characterization were used including thermal-optical transmission of OC, WSOC measurements, absorption measurements of water extractable OC, and radiocarbon (^{14}C) abundance measurements.

2. Materials and Methods

2.1. Sample Collection and Bulk Carbon Analysis

All samples were collected at the Department of Energy Atmospheric Radiation Measurement (ARM) Climate research facility (71°19′23.73″N, 156°36′56.70 W) on the North Slope of Alaska (NSA). The NSA-ARM facility, in operation since 1997, is located 7.4 km northeast of the village of Utqiaġvik, AK, 515 km north of the Arctic Circle.

PM_{10} samples were collected on quartz fiber filters (QFF, Tissuquartz™ Filters 2500 QAT-UP, 20 × 25 cm) using a Tisch high-volume PM_{10} sampler (Tisch Environmental, Cleves, OH, USA). $PM_{2.5}$ samples were collected on 90 mm QFFs (Pall Corporation, Ann Arbor, MI) using a URG medium volume $PM_{2.5}$ sampler (URG-3000b, URG Corporation, Research Triangle Park, NC). Prior to sampling, QFFs were baked at 500°C for 12 h and stored in baked aluminum foil packets and storage bags in a −10°C freezer prior to and post sampling. The duration was approximately 1 week per sample from June 2012 to June 2013. All blanks were treated in the same manner as samples. Samplers were located on a sampling platform approximately 10 m aboveground level.

OC and elemental carbon (EC) concentrations were determined using a thermal-optical transmission carbon analyzer (Sunset Laboratories, Tigard, OR) utilizing the NIOSH 5040 protocol [*Birch and Cary*, 1996]. Instrument blanks and sucrose standards were run with every batch of 10 samples, and all samples were blank subtracted using an average blank value of 0.18 μg OC cm^{-2}. Total organic carbon (TOC) is the sum of the OC and EC fractions for each sample. Following the nomenclature suggested by *Petzold et al*. [2013], BC will be used to refer to non-OC light-absorbing carbon with no reference to a specific measurement method, while EC will refer to the concentration of non-OC light-absorbing carbon evolved from the thermal-optical method mentioned above.

2.2. Water-Soluble Organic Carbon and Absorption Measurements

WSOC analysis was performed using a previously described method [*Barrett and Sheesley*, 2014]. Briefly, filter areas corresponding to ~75 μg of OC, based on filter loading, were placed in 50 mL centrifuge tubes (Bio-Link Scientific, Wimberly, TX) and sonicated in 30 mL of deionized (DI) water for 15 min. All tubes were precleaned by triple rinsing with DI water prior to extractions. The extracts were then centrifuged for 10 min and decanted. The sample is then split with 20 mL of the extract filtered into glass vials using precleaned disposable Millex® -GV syringe-driven filters (33 mm, pore size 0.22 μm; Merck Millipore, Ltd., Ireland). Forty microliters of 6N HCl was added to remove any CO_2 trapped in solution. WSOC concentrations were measured as dissolved OC in the solution using a Shimadzu total organic carbon [*Zaveri et al*., 2012] analyzer (TOC-5000A, Shimadzu, Kyoto, Japan). Samples were run with calibration standards (Potassium Hydrogen Phthalate, KHP, $C_8H_5KO_4$, Ultra Scientific, North Kingstown, RI) at 0, 0.5, 1, 2, 3, 4, and 5 mg L^{-1}, measured prior to analysis and periodically throughout each batch group. Samples were analyzed in triplicate (100 μL injection volume), and the reported value is the average of the three injections. All samples were blank subtracted using an average laboratory and field blank value of 0.26 mg L^{-1} prior to conversion to ambient concentrations. The remaining 10 mL of extract was filtered into a separate glass vial and reserved for absorption analysis.

Light absorption of the filtered aqueous extracts was measured from 300 to 700 nm on an Agilent 8453 ultraviolet-visible spectrometer (Santa Clara, CA), with tungsten and deuterium light sources, immediately following the water extraction process. Acidification was not applied to sample extracts used in light absorption measurements. Absorption spectrums were determined relative to a reference cuvette containing the same solvent [*Chen and Bond*, 2010]. The mass absorption efficiency (MAE) of water extracts was calculated for each WSOC sample using equation (1):

$$\mathrm{MAE}_\lambda = \frac{\mathrm{Abs}_\lambda}{[\mathrm{WSOC}]} = \frac{(\mathrm{ATN}_\lambda - \mathrm{ATN}_{700}) \times \frac{V_w}{V_a \times l} \times \ln(10)}{[\mathrm{WSOC}]} \quad (1)$$

where Abs_λ represents the light absorption coefficient (Mm^{-1}), [WSOC] represents the ambient WSOC concentration of the sample (μg m^{-3}), ATN_λ is the light attenuation at the given wavelength measured by the spectrophotometer, V_w is the volume of the water extract (mL), V_a is the air volume (m^3), and l is the optical path length (0.01 m) [*Yan et al*., 2015]. MAE was calculated at 365 nm in order to avoid possible interference from inorganic compounds as done with previous WSOC absorption studies. The wavelength (λ) dependence of WSOC absorption, the absorption Ångström exponent (AAE), was investigated by the following relationship:

$$\frac{A(\lambda_1)}{A(\lambda_2)} = \left(\frac{\lambda_2}{\lambda_1}\right)^{\mathrm{AAE}} \quad (2)$$

AAE was determined with a linear regression of ln (Abs_λ) against ln (λ) through the range of 330–400 nm, where the slope = −AAE (r^2 = 0.99 for all samples from this study; Figure S7 in the supporting information) [*Chen and Bond*, 2010; *Kirillova et al*., 2014; *Yan et al*., 2015].

2.3. Carbon Isotope Analysis and Radiocarbon Source Apportionment

In addition to characterizing the optical properties of OC, it is also of importance to determine the source contributions of OC to the Arctic. Often, source apportionment of OC in the Arctic has relied on a combination of elemental and organic tracers; however, due to uncertainty of the atmospheric lifetime of certain organic tracers at remote sites, the accuracy of this method is uncertain; therefore, ^{14}C abundance was used for source apportionment [*Barrett et al*., 2015; *Sheesley et al*., 2011; *Yttri et al*., 2014]. Due to the large difference in ^{14}C end-members for biogenic/biomass burning and fossil fuel combustion sources, apportionment between the contributions of fossil and contemporary carbon to OC with low uncertainty is possible [*Budhavant et al*., 2015; *Gustafsson et al*., 2009; *Lewis et al*., 2004; *Sheesley et al*., 2012]. Here contemporary carbon is defined as all OC derived from biogenic emissions and biomass combustion, including OC-derived secondary aerosol. Fossil carbon would include combustion and noncombustion, primary and secondary organic aerosol sources.

Ambient PM_{10} samples were composited to give ~60 μg of TOC [*Zaveri et al*., 2012] for accelerator mass spectrometry measurement of the ^{13}C and ^{14}C signals. Composites were optimized for EC loading, which will be presented in a future manuscript; individual samples not included in composites will undergo radiocarbon analysis in the future. Samples included in composites are shown in Tables S1 and S2 in the supporting informtion. The fall composite does not include samples with the highest OC concentrations due to the composites being optimized for EC loading. Samples were composited by 10 day back trajectory analysis (Table S1) with samples having similar air mass source region, and of the same season, composited together. For radiocarbon composites, each included sample was represented by equal mass of TOC. Therefore, the ^{14}C source apportionment is a true average of the included samples and not one individual sample is biasing the apportionment. TOC filter samples were acidified in a desiccator over HCl for 12 h to remove carbonate and then dried in a drying oven at 60°C for 1 h. Samples were then placed in prebaked glass petri dishes. ^{14}C abundance measurements were performed at the National Oceanic Sciences Accelerator Mass Spectrometry facility at Woods Hole Oceanographic Institute (Woods Hole, MA). Results are reported as fraction modern which is a measurement of the deviation of the $^{14}C/^{12}C$ ratio of a sample from the "modern reference, defined as 95% of the radiocarbon concentration in A.D. 1950 of NBS Oxalic Acid I.

In order to accurately apportion TOC based on ^{14}C abundance, $\Delta^{14}C$ end-members (standard values used to reference the radiocarbon abundance in the two source categories, fossil, and contemporary) must be defined and used in the following equation:

$$\Delta^{14}C_{\mathrm{TOC}} = \left(\Delta^{14}C_{\mathrm{contemporary}}\right)\left(F_{\mathrm{contemporary}}\right) + \left(\Delta^{14}C_{\mathrm{fossil}}\right)\left(1 - F_{\mathrm{contemporary}}\right) \quad (3)$$

The $\Delta^{14}C$ end-member for contemporary carbon (OC derived from biogenic emissions and biomass combustion) used was +107.5‰, based on wood burning from a 2010 reference from temperate regions [*Barrett et al*., 2015; *Zotter et al*., 2014]. The $\Delta^{14}C$ end-member for fossil fuels was −1000‰ [*Gustafsson et al*., 2009]. The contribution from fossil carbon is equal to $1 - F_{\mathrm{contemporary}}$, and $\Delta^{14}C$ of OC was calculated from $\Delta^{14}C_{\mathrm{TOC}}$ and $\Delta^{14}C_{\mathrm{EC}}$ using TOC = OC + EC [*Barrett et al*., 2015]. TOC uncertainty calculations include instrumental standard error, blank correction uncertainty, and end-member uncertainty. OC uncertainty calculations are based on a sensitivity analysis performed in order to account for the inadvertent inclusion of pyrolysis carbon with the EC fraction when isolating the EC fraction from OC. For the current study, sensitivity analysis indicates an average uncertainty of 9.8%. Further details on the sensitivity analysis protocol are included in *Barrett et al*. [2015] and *Chen et al*. [2013].

2.4. Normalization for Seasonal Analysis

Sample times ranged from 7 to 10 days throughout the year-round sampling campaign. In order to calculate seasonal averages despite the difference in sample duration, a normalization was applied based on sample duration [*Sheesley et al*., 2012]. The following equation was used to calculate averages based on sample duration (hours) which is a means of tracking sample duration:

$$C_j = (\Sigma_i C_i v_i)/(\Sigma v_i) \quad (4)$$

where C_i is the OC concentration for sample i, v_i is the sample duration for sample i, and C_j equals the normalized average concentration. The normalized concentrations are reported throughout the manuscript and also

used as input for source apportionment based on ^{14}C analysis. Seasonal and annual ^{14}C averages were normalized based on composite sample duration and concentration using the following equation:

$$F_j = (\Sigma_i C_i F_i t_i)/(\Sigma_i C_j t_i) \quad (5)$$

where F_i is the F_m for composite i, C_i is the normalized OC concentration for composite i, t_i is the sampling duration, and C_j is the normalized average concentration [*Sheesley et al*., 2012]. Seasonal averages were calculated based on the following seasonal definitions: summer (>15 h daylight), winter (<12 h daylight), and the transitional seasons of spring and fall with 12–15 h of daylight. This seasonal delineation differs from prior OC studies in the region which split the year into only three seasons: spring (March–June), summer (July–October), and winter (November–February) [*Shaw et al*., 2010].

2.5. Back Trajectory Analysis

Back trajectory analysis was completed using the National Oceanic and Atmospheric Administration Hybrid Single-Particle Lagrangian Integrated Trajectory (HYSPLIT) model, version 4 [*Draxler and Rolph*, 2010] in order to broadly identify potential source regions of OC to the North American Arctic. Briefly, 10 day back trajectories starting every 6 h were run for each sampling day during the study period. Further description of the model parameters is available in *Barrett et al*. [2015]. The resulting back trajectories were clustered for the time representing each filter sample using the clustering function available in the model. The results of this cluster analysis were used to group the filter samples for radiocarbon analysis into composites based on geographic source region by season. The cluster means were then mapped using Environmental Systems Research Institute ArcGIS 10 software. Due to the limited number of meteorological monitoring stations in the region, back trajectory models can be imprecise for this study area. A sensitivity analysis of back trajectories was conducted, and results show the model to be robust [*Barrett et al*., 2015]. Briefly, back trajectories were completed for two additional locations, as well as the sampling location, with three different starting heights (50, 100, and 500 m). Back trajectories from each location and starting height followed the same trends as the back trajectories used for this study. Here back trajectories are used only to provide a broad description of source regions to the sampling site.

3. Results

3.1. Back Trajectory Analysis Results

Cluster means representing 10 day back trajectories for each filter sample revealed five major source regions to Utqiaġvik, AK, throughout the study period: the Russian Arctic, Canadian Arctic, Alaskan Arctic, the Arctic Ocean, and western Alaska (Figures 1a–1d; back trajectories are colored by ^{14}C composite and depicted by season, two summer seasons are included, 2012 and 2013, and the dashed lines represent <10% of total back trajectories). A fraction of each trajectory has transit time over the Arctic Ocean in all sampled weeks, pointing to a potential marine/sea ice influence in OC in all seasons. Discussion will focus on the differences among seasonal back trajectory analysis.

Summer back trajectories mainly consisted of air masses originating along the Russian Arctic and western Alaska, with minor impact from the Canadian Arctic. Influence from interior and western Alaska increased into August 2012, while air masses from the Russian Arctic decreased. For the late summer, 12 through 31 August, back trajectories were dominated by interior Alaskan influence. Wildfires influencing the summer 2012 back trajectories are shown in Figure 1b; Alaskan wildfires accounted for just over 3% of the total acreage burned in the U.S. (http://activefiremaps.fs.fed.us/data/fireptdata/modisfire_2012_conus.htm). While the majority of the fires are to the east of the major back trajectory source regions, there were significant fires in the interior Alaskan source region.

For the fall, back trajectories shifted from western Alaska/Canadian Arctic to mainly the Russian Arctic as the major source region: 41% of back trajectories for the first week of fall, 21–28 September, passed over western Alaska; however, the influence of western Alaska decreases throughout the remainder of the season, with northern Alaska and the Russian Arctic as the major source regions to Utqiaġvik.

Winter back trajectories have been previously described by *Barrett et al*. [2015]. In the previous manuscript, back trajectories originating in both the Alaskan Arctic and the Canadian Arctic were combined and referred to as the North American Arctic; however, in this manuscript, we make the distinction between the two

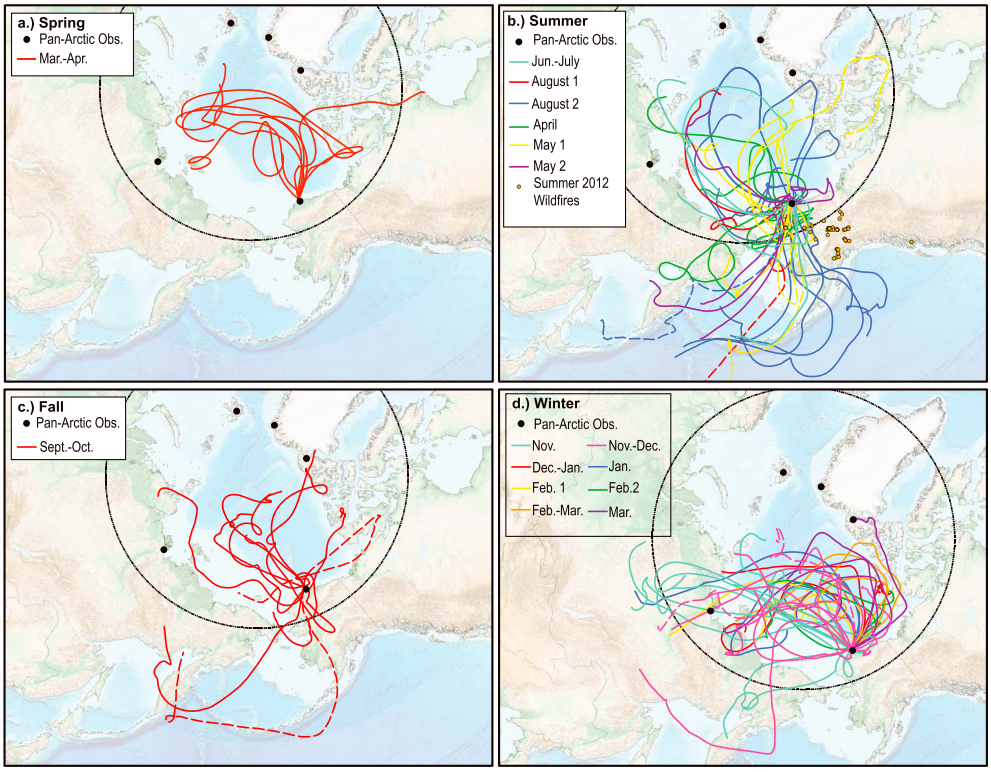

Figure 1. Ten-day back trajectory cluster means for (a) spring, (b) summer, (c) fall, and (d) winter for Utqiaġvik, AK. Back trajectories are colored according to composite for radiocarbon analysis with each line representing a cluster mean for each sample included in the composite. Date ranges for each composite are as follows: March–April: 20 March to 12 April 2013; June–July: 29 June to 30 July; 1 August: 3–12 August 2012; 2–8 to 31 August 2012; September–October: 7 September to 26 October 2012; November: 3–26 November 2012; November–December: 26 November to 21 December 2012; December–January: 28 December 2012 to 5 January 2013; January: 18–25 January 2013; 1 February: 1–8 February 2013; 2 February : 8–15 February 2013; February–March: 25 February to 1 March 2013; March: 1–11 March 2013; April: 12–26 April 2013; 1 May: 10–24 May 2013; 2 May: 27 May to 4 June 2013.

regions. Briefly, the winter is characterized by two major source regimes: the midwinter period with heavy influence from the Arctic Ocean and the Russian Arctic and a shift in the late winter to air masses spending time over the Canadian Arctic. This back trajectory analysis represents the current annual campaign but may not represent the long-term annual trends in source regions for the NSA.

During the sampling campaign, the meteorology of Utqiaġvik was influenced by both positive and negative phases of the Arctic Oscillation (AO) [*NOAA*, 2015]. The positive phase of the AO is expected to increase wind transport from North America and Europe into the Arctic [*Eckhardt et al*., 2003; *L'Heureux et al*., 2010; *Wu et al*., 2006]. The positive phase of the AO occurred from May through September 2012, with the exception of a negative phase during June 2012. A transition to the negative phase occurred in October 2012 persisting through March 2013. The strongest negative phase occurred in March 2013, prior to a return to the positive phase in April and May 2013. A negative phase of the AO during the winter would help isolate the region from emissions in the lower latitudes during this season, limiting the region to in-Arctic emissions.

3.2. Annual and Seasonal OC Trends

It is well known that aerosol pollution in the Arctic, specifically BC, peaks in the late winter and early spring periods when the polar dome traps pollutants over the Arctic, in a phenomenon known as Arctic Haze (as seen in Figures 1a and 1d, with most of the air masses originating within the Arctic) [*Law and Stohl*, 2007; *McNaughton et al*., 2011; *von Schneidemesser et al*., 2009; *Wang et al*., 2011]. EC concentrations at Utqiaġvik, AK (an operational definition of BC as measured by thermal optical techniques), during the sampling campaign follow established BC trends for the Arctic with elevated concentrations in the winter and spring and very low concentrations during the summer (Figure 2 and Table S2). Further discussion of the optical

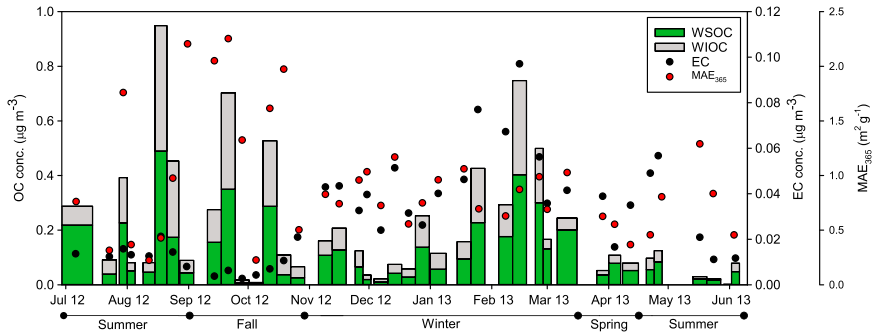

Figure 2. Year-round water-soluble organic carbon (WSOC), water-insoluble organic carbon (WIOC), elemental carbon (EC) concentrations, and mass absorption efficiency (MAE_{365}) values at 365 nm during the sampling campaign for Utqiaġvik, AK, from 2012 to 2013.

and source characteristics of EC will be presented in a future manuscript. Our annual campaign results indicate that seasonal OC trends do not always follow the same pattern as seasonal BC trends in the Arctic, with peaks in late summer (August) and early fall (September–October) in addition to the late winter (February–March) for 2012–2013. Ambient OC concentrations for the year range from 0.008 ± 0.002 μg m^{-3} to 0.95 ± 0.06 μg m^{-3} (Figure 2). Seasonal PM_{10} average OC burdens ranged from 0.08 ± 0.03 μg m^{-3} in the spring to 0.24 ± 0.27 μg m^{-3} in the fall (Table 1). A prior study from 1997 to 1999 in northern Finland found that OC concentrations peaked between July and September (concentrations reaching >1.5 μg m^{-3}), with concentrations decreasing to a background level 2 to 3 times lower than the summer maximum [*Ricard et al*., 2002]. OC concentrations during our campaign did have maximum concentrations occurring between July and September but had a second maximum in early February (0.75 ± 0.05 μg m^{-3}; Figure 2). WSOC and water-insoluble carbon (WIOC) also had a wide range with WSOC values ranging from 0.005 ± 0.004 μg m^{-3} to 0.49 ± 0.05 μg m^{-3} (Figure 2). WSOC had similar trends to OC, with maximum concentrations occurring July through September, and a second high period in winter. However, average summer WSOC (0.11 μg m^{-3}) is lower than previously reported WSOC values in Alert, Canada (0.19 μg m^{-3}, February to June 1991) [*Kawamura et al*., 2010], and aerosol phase WSOC for the summer 2006 at Summit, Greenland (0.19 ± 0.17 μg m^{-3}) [*Anderson et al*., 2008], as well as lower than the average WSOC summer concentration reported for 2009 in the Beaufort Sea (0.373 μg m^{-3}) [*Hu et al*., 2013]. On average, WSOC accounted for 57 ± 11% of the total OC burden throughout the sampling campaign, which is consistent with previous WSOC contributions. Average % WSOC values for our campaign are equivalent to average % WSOC in Alert, Canada, from February to June 1991 (56%) and similar to urban and rural values from the southeastern United States (51.9% and 55.8% annually) [*Zhang et al*., 2012]; however, % WSOC values in our study were much greater than values for the Maldives, a long-range transport site in the Indian Ocean, from 2008 to 2009 (15–29%) [*Kirillova et al*., 2013]. The spring transitional period accounted for the highest average WSOC/OC, 63% WSOC (although this is only 6% difference from the annual average), which may indicate the presence of aged aerosols at the site. The slight increase in the WSOC/OC ratio in the spring corresponds with a switch to the positive phase of the Arctic Oscillation, which may transport more aged aerosols to Utqiaġvik via long-range transport. In addition, studies of secondary organic acids, which include organic diacids, indicate peak secondary organic aerosol (SOA) production of these aerosols in late winter/early springtime and concurrent with Arctic haze [*Hansen et al*., 2014; *Kawamura et al*., 2005; *Nguyen et al*., 2014].

Prior to this campaign, there were limited studies of Arctic OC and WSOC in the North American Arctic; a previous study of organic functional groups indicated a mix of combustion and ocean-derived aerosols [*Shaw et al*., 2010]. Regression analysis of EC versus OC, EC versus WSOC, and EC versus WIOC show no correlation (Figures S1, S2, and S3), indicating different sources of EC compared to OC, WSOC, and WIOC during the sampling campaign. The lack of correlation between EC and OC indicates that OC is likely impacted by atmospheric processing (i.e., SOA growth) and noncombustion sources including secondary organic aerosol and biogenic emissions (which do not emit EC); this is further supported by a strong correlation between OC and WSOC (r^2 = 0.82; Figure S4). Studies also have shown that OC can have a shorter residence time than EC in the marine atmosphere [*Bosch et al*., 2014].

Table 1. Average Seasonal Concentrations(±SD) of Organic Carbon (OC), Water-Soluble Organic Carbon (WSOC), % WSOC, Mass Absorption Efficiency at 365 nm (MAE_{365}), Absorption Angstrom Exponent (AAE), and % Contemporary and Fossil Contributions to PM_{10} Aerosols From June 2012 to June 2013 in Utqiaġvik, AK

	Carbon Concentration			Optical Properties		Radiocarbon TOC[a]		Radiocarbon OC[b]	
Season	PM_{10} OC Conc. ± SD ($\mu g\ m^{-3}$)	PM_{10} WSOC ± SD ($\mu g\ m^{-3}$)	% WSOC /OC	PM_{10} MAE_{365} ± s.d. ($m^2\ g^{-3}$)	PM_{10} AAE ± SD	TOC % Contemporary ± Unc.	TOC % Fossil ± Unc.	OC % Contemporary ± Unc.	OC % Fossil ± Unc.
Summer	0.20 ± 0.26	0.11 ± 0.13	55%	0.70 ± 0.44	3.21 ± 1.78	62.4 ± 3.8	37.6 ± 3.8	64.8 ± 9.8	35.2 ± 9.8
Fall	0.24 ± 0.27	0.12 ± 0.14	50%	1.54 ± 0.75	3.39 ± 1.42				
Fall composite	0.05 ± 0.21	0.02 ± 0.12	37%	1.79 ± 0.41	3.01 ± 1.38	32.6 ± 3.8	67.4 ± 3.8	38.6 ± 9.8	61.4 ± 9.8
Winter	0.22 ± 0.19	0.13 ± 0.11	59%	0.82 ± 0.19	4.76 ± 2.28	50.6 ± 3.8	49.4 ± 3.8	50.3 ± 9.8	49.7 ± 9.8
Spring	0.08 ± 0.03	0.05 ± 0.02	63%	0.74 ± 0.25	2.91 ± 1.02	48.0 ± 3.8	52.0 ± 3.8	68.9 ± 9.8	31.1 ± 9.8

[a]Measured by ^{14}C.
[b]Calculated by subtraction of measured ^{14}C [*Barrett et al.*, 2015].

Maximum weekly OC concentrations occurred in the summer (0.95 ± 0.06 $\mu g\ m^{-3}$) possibly due to increased contribution from lower latitudes and interior Alaskan sources, including wildfires (Figure 1) and biogenic SOA combined with potential contribution from marine biogenic sources. However, the lack of correlation with EC and very low summer concentrations for EC make wildfire contribution less likely. Back trajectories for that period show consistent contribution from the Western interior of Alaska with periodic influence from the Arctic Ocean, including the Chukchi and Bering Seas, which exhibit higher biogenic activity [*Sharma et al.*, 2012]. In addition, the stable carbon (^{13}C) signature for the summer samples (Figure 3) has an enriched signal which may indicate contribution from marine sources or may indicate atmospheric processing [*Kirillova et al.*, 2013]. Atmospheric processing can affect the $\delta^{13}C$ signature through atmospheric oxidants preferentially reacting with lighter isotopes of VOCs which enriches the $\delta^{13}C$ signature in the residual VOCs and depletes the $\delta^{13}C$ of the particulate oxidation products. In contrast, photochemical aging of existing aerosol carbon would enrich the particulate phase. Ambient WSOC would be affected by these kinetic isotope effects [*Bosch et al.*, 2014; *Kirillova et al.*, 2013]. Marine OC can also be primary [*Gantt and Meskhidze*, 2013], which would include a combination of OC present in seawater as dissolved and particulate carbon.

Previous long-term studies of MSA concentrations at Utqiaġvik indicate periods of high concentration for April–August, which increased ~12% per year during the summer from 1997–2008, which aligns with our high OC concentrations in summer and supports our SOA and biogenic hypothesis [*Quinn et al.*, 2009]. If this trend continues into our sampling campaign, then MSA could contribute as much as 20% of the summer OC burden (based on the 2007 MSA concentration of 0.02 $\mu g\ m^{-3}$). However, synoptic measurement of MSA and OC is needed in this region. Results from the current study, combined with previous efforts indicate complexity with regard to OC sources in the Arctic. Therefore, continued long-term sample collection and modeling of functional

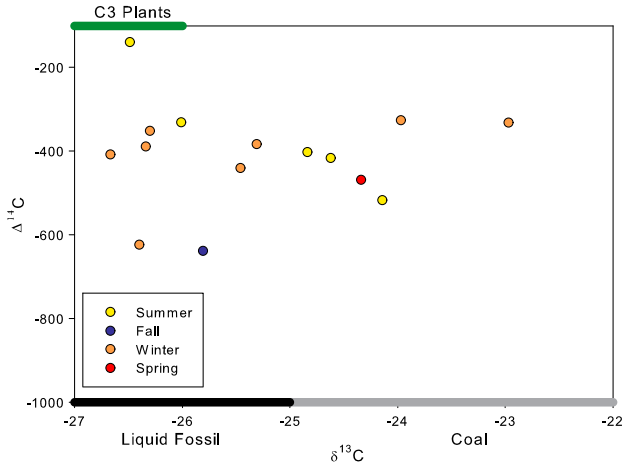

Figure 3. Scatterplot of ^{14}C and ^{13}C for total organic carbon (TOC) composites from Utqiaġvik, AK.

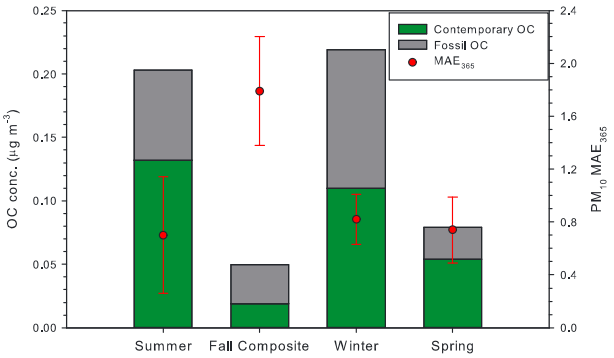

Figure 4. Seasonal PM_{10} OC contemporary and fossil concentrations and mass absorption efficiency (MAE) at 365 nm. % contemporary contributions are shown in green.

groups and specific organic acids used as SOA tracers in the region are needed for a better understanding of atmospheric processes affecting OC.

3.3. Radiocarbon Source Apportionment

Radiocarbon results indicate strong seasonal influences of fossil and contemporary carbon. Fossil carbon contributions to TOC (OC plus EC) averaged 51.6 ± 15.3% for the year, accounting for as much as 67.4 ± 3.8% in the fall (composite does not include select OC samples; Tables S1 and S2) and as little as 37.6 ± 3.8% of TOC in the summer (Figure 4 and Table 1). Increased fossil contributions in the fall are likely due to primary emissions or SOA resulting from liquid fossil and coal burning activity in the Arctic region from both the domestic and power generation sectors. A recent study of EC in the Siberian Arctic (Tiksi, Russia), which combined results from a dispersion model, emissions inventory, and observations (stable and radiocarbon), showed that liquid fossil and coal burning emission were the dominant sources of EC, which would be coemitted with OC; gas flaring is likely a minor fossil source in the region [*Winiger et al*., 2017]. Back trajectories from the Russian Arctic combined with stable carbon isotopic signatures from this study corroborate that liquid fossil and coal combustion are likely the main sources of OC during the fall composite in Utqiaġvik (Figures 1 and 3). Although stable carbon isotope signature can potentially be altered by atmospheric chemistry in the OC fraction, the results from the current study are quite different from gas flaring signatures ($\delta^{13}C$ −36 to −40).

For the entire sampling campaign (June 2012 to June 2013), the average fossil contribution to OC was 44.3 ± 9.8%; in other words, the OC is more contemporary than the EC. By season, fossil OC accounted for as much as 61.4 ± 9.8% in the fall to as little as 31.1 ± 9.8% and 35.2 ± 9.8% in the spring and summer, respectively (Table 1). Winter experienced relatively equal contributions between contemporary and fossil carbon (49.7 ± 9.8% fossil). Contemporary OC can result from primary and secondary biogenic carbon or biomass burning, including wildfire activity. One indication of biomass burning contribution is coemission of OC and EC, which occurs during most of the year. However, Figure 2 shows that EC is depleted during summer and early fall, while OC has several peak concentrations. Similarly, Figure 1 illustrates that back trajectories travel primarily to the west of wildfires which occurred in the eastern interior of Alaska, on the other side of the Brooks range. The sampling site in Utqiaġvik experienced a strong influence from the Arctic Ocean and the Alaskan coast (Figure 1), which would be source regions for primary and secondary marine and terrestrial biogenic emissions [*Kramshoj et al*., 2016]. The radiocarbon, OC:EC ratios, back trajectories, and wildfire data combine to suggest that the majority of contemporary OC in the Arctic summer resulted from biogenic emissions.

3.4. Optical Properties

PM_{10} MAE_{365} seasonal values ranged from 0.70 $m^2\ g^{-1}$ to 1.54 $m^2\ g^{-1}$ in the summer and fall, respectively, and average AAE values ranged from 2.91 ± 1.02 to 4.76 ± 2.28 in the spring and winter, respectively (Table 1 and Figure 4). AAE values among individual samples were variable during all seasons (Table S2), especially the summer season (55% relative standard deviation, RSD), while AAE values during the spring were the least variable (35% RSD). Absolute AAE values ranged from 1.35 to 6.37 in the summer and from 1.92 to 3.96 in the spring. Fall and winter had intermediate variability (42 and 49% RSD), with absolute values ranging from 1.43 to 4.73 in the fall and 1.83 to 9.59 during the winter (absolute values of AAE for all samples are available in the supporting information). Previous studies have shown AAE values ranging from 8.6 to 17.8 for woodsmoke, 5.2 to 8.8 for SOA, 4.8 for biomass smoke, and 6.1 for humic-like substances (HULIS) in Arctic snow [*Chen and Bond*, 2010; *Kirchstetter et al*., 2004; *Yan et al*., 2016]. Absolute AAE values can be used to help determine the contemporary carbon sources influencing the North American Arctic. Large winter AAE values would indicate a mixed source signal for contemporary BrC including woodsmoke and SOA, while lower AAE values in the summer and spring could possibly be due to increased biogenic OC contribution,

although specificity is difficult due to overlapping AAE value ranges from different contemporary sources. For individual winter samples with both AAE and ^{14}C analysis, the RSD for AAE values (36%) is greater than that of the RSD of the fraction fossil OC (9%), showing that AAE is much more variable than the fraction fossil of OC during the winter. These seasonal differences are particularly relevant in the Arctic where the incident radiation will vary so drastically; an annual average MAE will not accurately account for atmospheric radiative forcing in the summer (lowest MAE). PM_{10} MAE_{365} values are in good agreement with previously reported MAE values of 0.83 ± 0.15 m^2 g^{-1} and 0.27 ± 0.08 m^2 g^{-1}, at 470 and 530 nm wavelengths, respectively, in the western Arctic in 2008 [*McNaughton et al*., 2011]. The average MAE_{365} during the fall is significantly greater than all other seasons (p value < 0.001). Previous studies have indicated that WSOC emitted from biomass burning leads to higher MAE_{365} values [*Cheng et al*., 2011], but recently, it has been shown that solid fossil fuels, including lignite and high volatility bituminous coals (MAE_{OC} = 1.35 m^2 g^{-1}) can exhibit similar absorption in the near-UV range as biomass burning (i.e., woodsmoke) [*Olson et al*., 2015]. Fossil carbon contribution to OC was the highest in the fall composite (61.7 ± 9.8%) when the highest MAE_{365} values were observed, pointing to coal and liquid fuel as the major source of OC for samples included in the fall composite. Both primary emissions and secondary organic aerosols produced by burning coal will result in high MAE values [*Laskin et al*., 2015; *Lin et al*., 2015; *Nakayama et al*., 2013]. SOA produced from aromatic hydrocarbons emitted during combustion of liquid fossil fuels could also contribute to high MAE [*Lin et al*., 2015; *Liu et al*., 2015]. Samples not included in the fall composite exhibited both high and low MAE values (Table S2). These could be fossil or contemporary. Therefore, possible sources of OC based on MAE values for these samples could include coal combustion as well as humic-like substances (HULIS). Typically, HULIS is a result of biomass burning; however, recent studies show that HULIS can be produced through multiphase chemistry of anthropogenic and natural organic compounds, including fossil fuel combustion and biogenic and marine emissions [*Laskin et al*., 2015]. Therefore, the variable MAE_{365} exhibited in the fall samples not included in the composite could be due to a combination of primary emissions, SOA chromophores from aromatic VOCs, and HULIS derived from both anthropogenic and natural emissions. Additional radiocarbon analysis is needed for samples not included in the composite to confirm OC sources throughout the entire fall season. The seasons with the largest percent contributions from contemporary OC, spring and summer, exhibited the lowest average MAE_{365} values (Table 1). This is consistent with biogenic instead of biomass combustion sources dominating in spring and summer. Fall was also the most variable season, with a 50% RSD, while MAE_{365} values in the winter and spring were more consistent. In order to compare BC light absorption coefficient (b_{abs}) at 678 nm (λ of laser in Sunset OCEC carbon analyzer) with light absorption by BrC at 365 nm, the light absorption coefficient of BC at 365 was calculated using the power law wavelength dependence of b_{abs}, using AAE_{BC} = 1 [*Kirillova et al*., 2016]. Annually, WSOC BrC absorbs on average 3.4% relative to BC, ranging from 2.1% to 5.0% in the winter and summer respectively. However, there is uncertainty in the relationship between BrC absorption in bulk solutions and in aerosol; Liu et al. demonstrated aerosol measurement of b_{abs} BrC to be 2 times greater than b_{abs} BrC for a bulk solution [*Liu et al*., 2013]. OC mass concentrations can be up to 2 orders of magnitude greater than BC concentrations in the Arctic; therefore, the overall contribution of BrC to light absorption at 365 could be greater than that of BC on a mass concentration basis during low BC seasons. Globally, the radiative forcing of BrC is estimated to be 25% of that of BC [*Wu et al*., 2016]. For light absorption in North American snow, it has been proposed that HULIS and polar organic carbon account for 13% of the total light absorption [*Dang and Hegg*, 2014] and that BrC accounts for as much as 40% of total light absorption in Arctic snow [*Doherty et al*., 2010]. A recent study in the high Himalayas estimates that water soluble BrC absorption is 8 ± 1% of the light absorption of BC [*Kirillova et al*., 2016]. MAE_{365} measurements show that BrC is present in Utqiaġvik in all seasons and will contribute to the overall radiative balance of the region; any underestimation of this contribution will lead to inaccurate warming in climate models for the region. Previous laboratory studies of BrC resulting from wood combustion show that absorption over a bright surface (i.e., snow and ice) results in positive forcing values ranging from 6.3 to 23 W g^{-1}; however, additional modeling would be necessary to accurately determine the forcing of BrC absorption in a region such as the Arctic [*Chen and Bond*, 2010].

4. Conclusions

This study provides the first year-round data set for OC, WSOC, MAE_{365}, ^{13}C, and ^{14}C of TOC and OC for the North American Arctic region. OC concentrations did not follow the well-established seasonal trends for

Arctic BC. The peak concentrations for OC were seen in the summer, fall, and winter months, similar to a study from the late 1990s in Finland [*Ricard et al*., 2002]. WSOC also peaked in the summer, fall, and winter; however, the spring had the highest percent WSOC (63%), which potentially points to aged aerosols and SOA production influencing Utqiaġvik during this time. The fall had the highest average OC concentrations, and the fall composite exhibited the highest MAE_{365} values, coinciding with the highest contribution of fossil sources to OC at 61.4 ± 9.8%. The combination of $\delta^{13}C$ isotope signatures, back trajectories, and high MAE_{365} values point toward coal and liquid fossil fuel combustion as the major sources of OC during the fall composite. ^{14}C analysis results showed greater contributions of fossil carbon than contemporary carbon to TOC (both the OC and EC fractions) for the fall and minimum contributions of fossil carbon in the summer, while contributions of fossil and contemporary carbon were approximately even during the winter and spring. This summer high in contemporary OC is possibly due to the influence of secondary and biogenic sources of OC, which would not be seen in the EC fraction. Future studies with higher time resolution and additional chemical characterization are needed in order to further understand these contemporary biogenic and biomass combustion OC sources.

Acknowledgments

Financial and technical support for this campaign was provided by the United States Department of Energy (Atmospheric Radiation Measurement Field Campaign no. 2010-05876), NOAA (award no. NA14OAR4310150) and the C. Gus Glasscock, Jr. Endowed Fund for Excellence in Environmental Sciences. We would like to thank Dr. George Cobb and Baylor University for use of the PM_{10} sampler. We would also like to thank Walter Brower and Jimmy Ivanoff of the Ukpeagvik Inupiat Corporation for sample collection and field assistance as well as Fred Helsel, Dan Lucero, and Jeffrey Zirzow and the Sandia National Laboratory for site access and preparation. We would also like to thank Dr. Jeffrey A. Back and the Baylor University Center for Reservoir and Aquatic Systems Research for assistance with WSOC analysis. All results presented can be found in the supporting information.

References

Anderson, C., J. E. Dibb, R. J. Griffin, and M. H. Bergin (2008), Simultaneous measurements of particulate and gas-phase water-soluble organic carbon concentrations at remote and urban-influenced locations, *Geophys. Res. Lett.*, *35*, L13706, doi:10.1029/2008GL033966.

Bahadur, R., P. S. Praveen, Y. Xu, and V. Ramanathan (2012), Solar absorption by elemental and brown carbon determined from spectral observations, *Proc. Natl. Acad. Sci. U.S.A.*, *109*(43), 17366–17371.

Barrett, T. E., and R. J. Sheesley (2014), Urban impacts on regional carbonaceous aerosols: Case study in central Texas, *J. Air Waste Manag. Assoc.*, *64*(8), 917–926.

Barrett, T. E., E. M. Robinson, S. Usenko, and R. J. Sheesley (2015), Source contributions to wintertime elemental and organic carbon in the western Arctic based on radiocarbon and tracer apportionment, *Environ. Sci. Technol.*, *49*(19), 11631–11639.

Birch, M. E., and R. A. Cary (1996), Elemental carbon-based method for monitoring occupational exposures to particulate diesel exhaust, *Aerosol Sci. Technol.*, *25*(3), 221–241.

Bodhaine, B. A. (1995), Aerosol absorption measurements at Barrow, Mauna Loa and the south pole, *J. Geophys. Res.*, *100*(D5), 8967–8975.

Bosch, C., A. Andersson, E. N. Kirillova, K. Budhavant, S. Tiwari, P. S. Praveen, L. M. Russell, N. D. Beres, V. Ramanathan, and Ö. Gustafsson (2014), Source-diagnostic dual-isotope composition and optical properties of water-soluble organic carbon and elemental carbon in the South Asian outflow intercepted over the Indian Ocean, *J. Geophys. Res. Atmos.*, *119*, 11,743–11,759, doi:10.1002/2014JD022127.

Budhavant, K., A. Andersson, C. Bosch, M. Krusa, E. N. Kirillova, R. J. Sheesley, P. D. Safai, P. S. P. Rao, and O. Gustafsson (2015), Radiocarbon-based source apportionment of elemental carbon aerosols at two South Asian receptor observatories over a full annual cycle, *Environ. Res. Lett.*, *10*(2015), 064004.

Chen, B., et al. (2013), Source forensics of black carbon aerosols from China, *Environ. Sci. Technol.*, *47*(16), 9102–9108.

Chen, Y., and T. C. Bond (2010), Light absorption by organic carbon from wood combustion, *Atmos. Chem. Phys.*, *10*(4), 1773–1787.

Cheng, Y., et al. (2011), Mass absorption efficiency of elemental carbon and water-soluble organic carbon in Beijing, China, *Atmos. Chem. Phys.*, *11*(22), 11497–11510.

Dang, C., and D. A. Hegg (2014), Quantifying light absorption by organic carbon in Western North American snow by serial chemical extractions, *J. Geophys. Res. Atmos.*, *119*, 10,247–10,261, doi:10.1002/2014JD022156.

Delene, D. J., and J. A. Ogren (2002), Variability of aerosol optical properties at four North American surface monitoring sites, *J. Atmos. Sci.*, *59*(6), 1135–1150.

Doherty, S. J., S. G. Warren, T. C. Grenfell, A. D. Clarke, and R. E. Brandt (2010), Light-absorbing impurities in Arctic snow, *Atmos. Chem. Phys.*, *10*(23), 11647–11680.

Draxler, R. R., and G. D. Rolph (2010), HYSPLIT (HYbrid Single-Particle Lagrangian Integrated Trajectory) model access via NOAA ARL READY website (http://ready.Arl.Noaa.Gov/HYSPLIT.Php), edited, NOAA Air Resour. Lab., Silver Spring, Md.

Eckhardt, S., A. Stohl, S. Beirle, N. Spichtinger, P. James, C. Forster, C. Junker, T. Wagner, U. Platt, and S. G. Jennings (2003), The North Atlantic Oscillation controls air pollution transport to the Arctic, *Atmos. Chem. Phys.*, *3*(5), 1769–1778.

Eleftheriadis, K., S. Vratolis, and S. Nyeki (2009), Aerosol black carbon in the European Arctic: Measurements at Zeppelin station, Ny-Alesund, Svalbard from 1998-2007, *Geophys. Res. Lett.*, *36*, L02809, doi:10.1029/2008GL035741.

Feng, Y., V. Ramanathan, and V. R. Kotamarthi (2013), Brown carbon: A significant atmospheric absorber of solar radiation?, *Atmos. Chem. Phys.*, *13*(17), 8607–8621.

Gantt, B., and N. Meskhidze (2013), The physical and chemical characteristics of marine primary organic aerosol: A review, *Atmos. Chem. Phys.*, *13*(8), 3979–3996.

Gustafsson, O., M. Krusa, Z. Zencak, R. J. Sheesley, L. Granat, E. Engstrom, P. S. Praveen, P. S. P. Rao, C. Leck, and H. Rodhe (2009), Brown clouds over South Asia: Biomass or fossil fuel combustion?, *Science*, *323*(5913), 495–498.

Hansen, A. M. K., et al. (2014), Organosulfates and organic acids in Arctic aerosols: Speciation, annual variation and concentration levels, *Atmos. Chem. Phys.*, *14*(15), 7807–7823.

Hirdman, D., H. Sodemann, S. Eckhardt, J. F. Burkhart, A. Jefferson, T. Mefford, P. K. Quinn, S. Sharma, J. Strom, and A. Stohl (2010), Source identification of short-lived air pollutants in the Arctic using statistical analysis of measurement data and particle dispersion model output, *Atmos. Chem. Phys.*, *10*(2), 669–693.

Hu, Q.-H., Z.-Q. Xie, X.-M. Wang, H. Kang, and P. Zhang (2013), Levoglucosan indicates high levels of biomass burning aerosols over oceans from the Arctic to Antarctic, *Sci. Rep.*, *3*, 3119.

Kawamura, K., Y. Imai, and L. A. Barrie (2005), Photochemical production and loss of organic acids in high Arctic aerosols during long-range transport and polar sunrise ozone depletion events, *Atmos. Environ.*, *39*(4), 599–614.

Kawamura, K., H. Kasukabe, and L. A. Barrie (2010), Secondary formation of water-soluble organic acids and α-dicarbonyls and their contributions to total carbon and water-soluble organic carbon: Photochemical aging of organic aerosols in the Arctic spring, *J. Geophys. Res.*, *115*, D21306, doi:10.1029/2010JD014299.

Kirchstetter, T. W., T. Novakov, and P. V. Hobbs (2004), Evidence that the spectral dependence of light absorption by aerosols is affected by organic carbon, *J. Geophys. Res.*, *109*, D21208, doi:10.1029/2004JD004999.

Kirillova, A., R. Andersson, J. Sheesley, M. Kruså, P. S. Praveen, K. Budhavant, P. D. Safai, P. S. P. Rao, and Ö. Gustafsson (2013), 13C- and14C-based study of sources and atmospheric processing of water-soluble organic carbon (WSOC) in South Asian aerosols, *J. Geophys. Res. Atmos.*, *118*, 614–626, doi:10.1002/jgrd.50130.

Kirillova, E. N., A. Andersson, J. Han, M. Lee, and O. Gustafsson (2014), Sources and light absorption of water-soluble organic carbon aerosols in the outflow from northern China, *Atmos. Chem. Phys.*, *14*(3), 1413–1422.

Kirillova, E. N., A. Marinoni, P. Bonasoni, E. Vuillermoz, M. C. Facchini, S. Fuzzi, and S. Decesari (2016), Light absorption properties of brown carbon in the high Himalayas, *J. Geophys. Res. Atmos.*, *121*, 9621–9639, doi:10.1002/2016JD025030.

Kramshoj, M., I. Vedel-Petersen, M. Schollert, A. Rinnan, J. Nymand, H. Ro-Poulsen, and R. Rinnan (2016), Large increases in Arctic biogenic volatile emissions are a direct effect of warming, *Nat. Geosci.*, *9*(5), 349–352.

L'Heureux, M., A. Butler, B. Jha, A. Kumar, and W. Q. Wang (2010), Unusual extremes in the negative phase of the Arctic Oscillation during 2009, *Geophys. Res. Lett.*, *37*, L10704, doi:10.1029/2010GL043338.

Laskin, A., J. Laskin, and S. A. Nizkorodov (2015), Chemistry of atmospheric brown carbon, *Chem. Rev.*, *115*(10), 4335–4382.

Law, K. S., and A. Stohl (2007), Arctic air pollution: Origins and impacts, *Science*, *315*(5818), 1537–1540.

Lewis, C. W., G. A. Klouda, and W. D. Ellenson (2004), Radiocarbon measurement of the biogenic contribution to summertime PM-2.5 ambient aerosol in Nashville, TN, *Atmos. Environ.*, *38*(35), 6053–6061.

Li, C., P. Chen, S. Kang, F. Yan, Z. Hu, B. Qu, and M. Sillanpää (2016), Concentrations and light absorption characteristics of carbonaceous aerosol in PM2.5 and PM10 of Lhasa city, the Tibetan Plateau, *Atmos. Environ.*, *127*, 340–346.

Lin, P., J. Liu, J. E. Shilling, S. M. Kathmann, J. Laskin, and A. Laskin (2015), Molecular characterization of brown carbon (BrC) chromophores in secondary organic aerosol generated from photo-oxidation of toluene, *Phys. Chem. Chem. Phys.*, *17*(36), 23312–23325.

Liu, J., M. Bergin, H. Guo, L. King, N. Kotra, E. Edgerton, and R. Weber (2013), Size-resolved measurements of brown carbon in water and methanol extracts and estimates of their contribution to ambient fine-particle light absorption, *Atmos. Chem. Phys.*, *13*(24), 12389–12404.

Liu, P. F., N. Abdelmalki, H. M. Hung, Y. Wang, W. H. Brune, and S. T. Martin (2015), Ultraviolet and visible complex refractive indices of secondary organic material produced by photooxidation of the aromatic compounds toluene and m-xylene, *Atmos. Chem. Phys.*, *15*(3), 1435–1446.

McNaughton, C. S., et al. (2011), Absorbing aerosol in the troposphere of the Western Arctic during the 2008 ARCTAS/ARCPAC airborne field campaigns, *Atmos. Chem. Phys.*, *11*(15), 7561–7582.

Nakayama, T., K. Sato, Y. Matsumi, T. Imamura, A. Yamazaki, and A. Uchiyama (2013), Wavelength and NO x dependent complex refractive index of SOAs generated from the photooxidation of toluene, *Atmos. Chem. Phys.*, *13*(2), 531–545.

Nguyen, Q. T., T. B. Kristensen, A. M. K. Hansen, H. Skov, R. Bossi, A. Massling, L. L. Sorensen, M. Bilde, M. Glasius, and J. K. Nojgaard (2014), Characterization of humic-like substances in Arctic aerosols, *J. Geophys. Res. Atmos.*, *119*, 5011–5027, doi:10.1002/2013JD020144.

NOAA (2015), *Daily Arctic Osciallation Index, Edited*.

Olson, M. R., M. V. Garcia, M. A. Robinson, P. Van Rooy, M. A. Dietenberger, M. Bergin, and J. J. Schauer (2015), Investigation of black and brown carbon multiple-wavelength-dependent light absorption from biomass and fossil fuel combustion source emissions, *J. Geophys. Res. Atmos.*, *120*, 6682–6697, doi:10.1002/2014JD022970.

Petzold, A., et al. (2013), Recommendations for reporting "black carbon" measurements, *Atmos. Chem. Phys.*, *13*(16), 8365–8379.

Quinn, P. K., T. S. Bates, K. Schulz, and G. E. Shaw (2009), Decadal trends in aerosol chemical composition at Barrow, Alaska: 1976-2008, *Atmos. Chem. Phys.*, *9*(22), 8883–8888.

Ricard, V., J. L. Jaffrezo, V. M. Kerminen, R. E. Hillamo, M. Sillanpaa, S. Ruellan, C. Liousse, and H. Cachier (2002), Two years of continuous aerosol measurements in northern Finland, *J. Geophys. Res.*, *107*(D11), ACH 10-11–ACH 10-17, doi:10.1029/2001JD000952.

Sharma, S., D. Lavoue, H. Cachier, L. A. Barrie, and S. L. Gong (2004), Long-term trends of the black carbon concentrations in the Canadian Arctic, *J. Geophys. Res.*, *109*, D15203, doi:10.1029/2003JD004331.

Sharma, S., E. Andrews, L. A. Barrie, J. A. Ogren, and D. Lavoue (2006), Variations and sources of the equivalent black carbon in the high Arctic revealed by long-term observations at Alert and Barrow: 1989–2003, *J. Geophys. Res.*, *111*, D14208, doi:10.1029/2005JD006581.

Sharma, S., et al. (2012), Influence of transport and ocean ice extent on biogenic aerosol sulfur in the Arctic atmosphere, *J. Geophys. Res.*, *117*, D12209, doi:10.1029/2011JD017074.

Sharma, S., M. Ishizawa, D. Chan, D. Lavoue, E. Andrews, K. Eleftheriadis, and S. Maksyutov (2013), 16-year simulation of Arctic black carbon: Transport, source contribution, and sensitivity analysis on deposition, *J. Geophys. Res. Atmos.*, *118*, 943–964, doi:10.1029/2012JD017774.

Shaw, P. M., L. M. Russell, A. Jefferson, and P. K. Quinn (2010), Arctic organic aerosol measurements show particles from mixed combustion in spring haze and from frost flowers in winter, *Geophys. Res. Lett.*, *37*, L10803, doi:10.1029/2010GL042831.

Sheesley, R. J., A. Andersson, and O. Gustafsson (2011), Source characterization of organic aerosols using Monte Carlo source apportionment of PAHs at two South Asian receptor sites, *Atmos. Environ.*, *45*(23), 3874–3881.

Sheesley, R. J., E. Kirillova, A. Andersson, M. Krusa, P. S. Praveen, K. Budhavant, P. D. Safai, P. S. P. Rao, and O. Gustafsson (2012), Year-round radiocarbon-based source apportionment of carbonaceous aerosols at two background sites in South Asia, *J. Geophys. Res.*, *117*, D10202, doi:10.1029/2011JD017161.

Srinivas, B., and M. M. Sarin (2014), Brown carbon in atmospheric outflow from the Indo-Gangetic Plain: Mass absorption efficiency and temporal variability, *Atmos. Environ.*, *89*, 835–843.

von Schneidemesser, E., J. J. Schauer, G. S. W. Hagler, and M. H. Bergin (2009), Concentrations and sources of carbonaceous aerosol in the atmosphere of Summit, Greenland, *Atmos. Environ.*, *43*(27), 4155–4162.

Wang, Q., et al. (2011), Sources of carbonaceous aerosols and deposited black carbon in the Arctic in winter-spring: Implications for radiative forcing, *Atmos. Chem. Phys.*, *11*(23), 12453–12473.

Winiger, P., et al. (2017), Siberian Arctic black carbon sources constrained by model and observation, *PNAS*, *114*(7), E1054–E1061.

Wu, A., W. Hsieh, A. Shabbar, G. Boer, and F. Zwiers (2006), The nonlinear association between the Arctic Oscillation and North American winter climate, *Clim. Dyn.*, *26*(7–8), 865–879.

Wu, G.-M., Z.-Y. Cong, S.-C. Kang, K. Kawamura, P.-Q. Fu, Y.-L. Zhang, X. Wan, S.-P. Gao, and B. Liu (2016), Brown carbon in the cryosphere: Current knowledge and perspective, *Adv. Clim. Change Res.*, *7*(1–2), 82–89.

Yan, C. Q., et al. (2015), Chemical characteristics and light-absorbing property of water-soluble organic carbon in Beijing: Biomass burning contributions, *Atmos. Environ.*, *121*, 4–12.

Yan, F., S. Kang, C. Li, Y. Zhang, X. Qin, L. Yang, X. Zhang, Z. Hu, P. Chen, and X. Li (2016), Concentration, sources and light absorption characteristics of dissolved organic carbon on a medium-sized valley glacier, northern Tibetan Plateau, *Cryosphere*, *10*(6), 2611.

Yttri, K. E., C. L. Myhre, S. Eckhardt, M. Fiebig, C. Dye, D. Hirdman, J. Strom, Z. Klimont, and A. Stohl (2014), Quantifying black carbon from biomass burning by means of levoglucosan - a one-year time series at the Arctic observatory Zeppelin, *Atmos. Chem. Phys.*, *14*(12), 6427–6442.

Zaveri, R. A., et al. (2012), Overview of the 2010 carbonaceous aerosols and radiative effects study (CARES), *Atmos. Chem. Phys.*, *12*(16), 7647–7687.

Zhang, X., Z. Liu, A. Hecobian, M. Zheng, N. H. Frank, S. Edgerton, and R. J. Weber (2012), Spatial and seasonal variations of fine particle water-soluble organic carbon (WSOC) over the southeastern United States: Implications for secondary organic aerosol formation, *Atmos. Chem. Phys.*, *12*(14), 6593–6607.

Zotter, P., et al. (2014), Diurnal cycle of fossil and nonfossil carbon using radiocarbon analyses during CalNex, *J. Geophys. Res. Atmos.*, *119*, 6818–6835, doi:10.1002/2013JD021114.

Erratum

In the originally published version of this article, the grant number for one of the funding agencies was missing from the acknowledgments section. The error has since been corrected and this version may be considered the authoritative version of record.